James R. Reeder[1]

A Criterion to Control Nonlinear Error in the Mixed-Mode Bending Test

Reference: Reeder, J. R., **"A Criterion to Control Nonlinear Error in the Mixed-Mode Bending Test,"** *Composite Materials: Testing and Design Fourteenth Volume, ASTM STP 1436,* C. E. Bakis, Ed., American Society for Testing and Materials, West Conshohocken, PA, 2003.

Abstract: The mixed-mode bending test has been widely used to measure delamination toughness and was recently standardized by ASTM as Standard Test Method D6671-01. This simple test is a combination of the standard Mode I (opening) test and a Mode II (sliding) test. This test uses a unidirectional composite test specimen with an artificial delamination subjected to bending loads to characterize when a delamination will extend. When the displacements become large, the linear theory used to analyze the results of the test yields errors in the calculated toughness values. The current standard places no limit on the specimen loading and therefore test data can be created using the standard that are significantly in error. A method of limiting the error that can be incurred in the calculated toughness values is needed. In this paper, nonlinear models of the MMB test are refined. One of the nonlinear models is then used to develop a simple criterion for prescribing conditions where the nonlinear error will remain below 5%.

Keywords: Delamination, mixed-mode, composite, nonlinear, MMB test, toughness

Nomenclature

a	Crack length
b	Specimen width
c	Lever length
h	Half thickness of the specimen
h^*	Hinge height
m,n,q	nondimensionalized parameters defined in the KIN model
L	Half span length of the MMB apparatus
E	Extensional modulus
EI	Bending stiffness of half-thickness beam
F	Applied moment correction parameter from the KIN model
G	Strain energy release rate
G_{12}	Shear modulus
P	Load reacted on the MMB specimen
$P_{applied}$	Applied load to the MMB apparatus
V	Height of applied load location

[1]NASA Langley Research Center, Hampton VA, 23681-2199.

X, Y	The location of a point in the local coordinate system
α	Rotation of a point on the test specimen (in the global coordinate system)
δ	displacement at the applied load point
δ_{ab}	displacement at hinged end of specimen
η	Scaling term for deformation base on individual modes
θ_o	Rotation of crack tip (and therefore the local coordinate system)
θ_L	Rotation of the lever in the global coordinate system
ξ	defined correction parameters from the KIN model
ϕ	Slope of the test specimen at a point (in local coordinate system)
χ	Crack length correction factor
Γ	anisotropy factor
Δ	Change in parameter causing nonlinearity

Superscript

A,B,C,D,O	Parameter pertaining to a given location on the specimen
F	Parameter pertaining to the applied loading location on the MMB fixture

Subscript

11,22,12	Pertaining to the longitudinal, transverse, and shear, respectively
I, II	Pertaining to Mode I or Mode II
a	Pertaining to the top lever arm
b	Pertaining to the bottom lever arm
est	estimated value
T	Pertaining to the combined Mode I and Mode II strain energy release rate
X,Y	Parameter expressed in the local coordinate system
XX, YY	Parameter expressed in the global coordinate system

Parameter Definitions

$$EI \equiv E_{11}\frac{bh^3}{12} \qquad \Gamma \equiv 1.18\frac{\sqrt{E_{11}E_{22}}}{G_{13}} \qquad \chi \equiv \sqrt{\frac{E_{11}}{11G_{12}}\left(3-2\left(\frac{\Gamma}{1+\Gamma}\right)^2\right)}$$

$$\eta_I \equiv \frac{(a+\chi h)^3}{a^3} \qquad \eta_{II} \equiv \frac{2L^3+3(a+0.42\chi h)^3}{2L^3+3a^3}$$

$$G_T \equiv G_I + G_{II} \qquad \frac{G_{II}}{G_T} \equiv \frac{G_{II}}{G_I+G_I}$$

Introduction

The mixed-mode bending (MMB) test shown in Figure 1 combines the double cantilever beam (DCB) test which is the standard test for Mode I toughness, with the end notched flexure (ENF) test[*1*] for Mode II toughness. This test was standardized by ASTM in 2001 as the Test Method for Mixed Mode I-Mode II Interlaminar Fracture Toughness of Unidirectional Fiber Reinforced Polymer Composite (D 6671). Although originally designed to test the static delamination toughness of composites, researchers

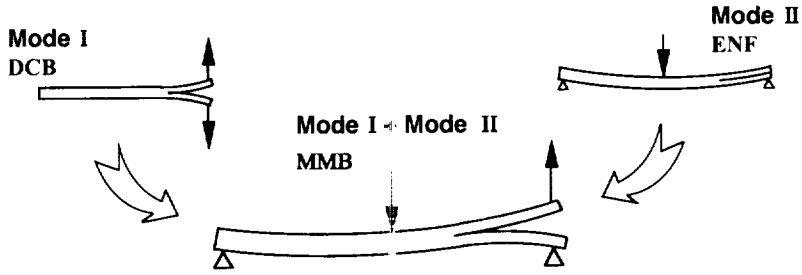

Figure 1—*Superposition of loading modes*

have extended the use of the MMB test to fatigue loading[*2,3*] and to toughness testing of adhesives[*4*].

The two loads shown in Figure 1, which are reacted on the MMB specimen are applied using a lever so that only one applied load is required. The ratio of the two loads and therefore the proportion of Mode I and Mode II loading is controlled varying the length of the lever arm. The advantages of the MMB test over other mixed-mode tests include: (1) the use of a single test specimen configuration to test over almost the entire range of Mode I to Mode II ratios, (2) a closed form model that is used to calculate the toughness values from measured quantities, and (3) a mixed-mode ratio that remains essentially constant during delamination growth[*5*]. The original MMB fixture showed a nonlinearity in the loading curve due to the rotation of the lever. This nonlinearity caused significant errors in the calculated toughness values and changed the mixed-mode ratio. This problem was largely alleviated by changing the way in which the lever was loaded[*6,7*]. The modified MMB apparatus, shown in Figure 2, loads the lever slightly above the midplane of the specimen using a saddle/yoke configuration. This loading height was optimized to reduce the nonlinear errors. The dramatic drop in the nonlinear error due to this modification in loading arrangement was confirmed by an independent analysis on a fatigue version of the MMB apparatus[*8*]. Although this redesign dramatically reduced the nonlinear effect, errors could still become significant if the loading was large enough[*9*].

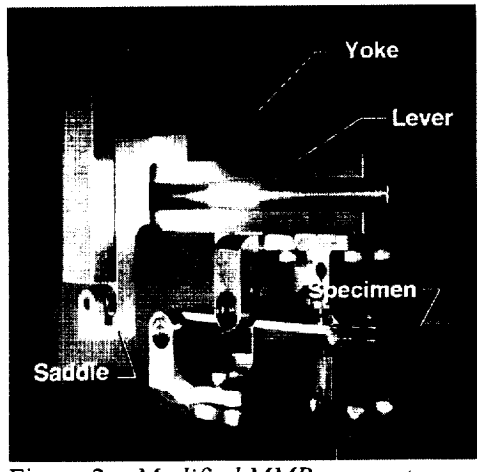

Figure 2—*Modified MMB apparatus*

The nonlinear errors found when loading becomes large come from many different sources. The most significant sources are shown schematically in Figure 3. The first source of error is caused by the crack length becoming shorter due to large bending deflections of the specimen. This change in apparent crack length causes the applied moment at the crack tip to be less than expected because the moment arm to the loads at the split end of the specimen are reduced. The calculated toughness therefore

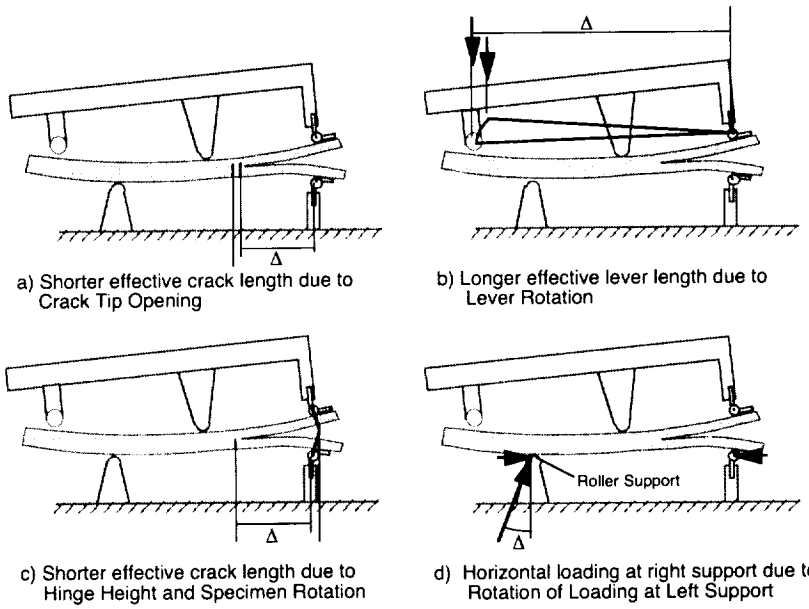

Figure 3—*Sources of nonlinear error*

over predicts that which was actually seen by the test specimen.

The second source of error, shown in Figure 3b, is due to the lever arm changing with deformation. This changes the moment that is applied to the specimen by the lever. Because the lever loading point begins slightly above the hinge point, the moment arm initially increases, but it can eventually drop below its original value. This change in the lever length can also cause the mixed-mode ratio to change.

The third source of error is a shortening of the crack length. Unlike the first source, this shortening of the crack length is due to the rotation of the specimen where the hinges attach. Because the hinges are offset from the center line of specimen rotation, the rotation causes the load point of the hinge to shift horizontally thus reducing the moment arm of the specimen and consequently the moment loading on the crack tip.

A fourth source of nonlinear error is shown in Figure 3d. This error is caused by the roller loading at the end opposite the hinges. As the specimen bends, the slope of the specimen at the roller changes. Since the loading is through a roller, it remains perpendicular to the surface of the specimen and a horizontal load component develops. Since no horizontal load is applied to the lever, the horizontal load from the base roller must be reacted by the hinge that is also attached to the base. This horizontal load on the base hinge increases the moment at the crack tip and shifts the mixed-mode ratio. A similar error is also created by the reaction of the roller in the center of the specimen, however the rotation of the specimen in the center is much smaller than that at the end so this error is negligible.

Because of all these sources for nonlinearity, estimating the error in using a linear MMB data reduction is complicated. The true toughness can be greater than or less than the apparent toughness. The nonlinear effects can also change the mixed-mode ratio. It

is important that these sources of nonlinear error be controlled in some way so that erroneous data is not generarted.

Kinloch et al. [*10*] proposed a method of correcting for the nonlinear error based on nonlinear correction proposed by Williams[*11*] for this type of bending specimen. This method only corrected for the nonlinear error associated with crack length shortening (source 1 shown in Figure 3a). The method calls for estimating the shortening of the crack length based on measurements of the opening displacement between loading hinges. A correction to the toughness value calculated from linear theory could then be made.

Sainath[*9*] used this correction when analyzing test data from T800H/3900-2 composite material. This material is quite tough so the applied loading in these tests was quite high. For such a tough material, the calculated delamination fracture toughness from the linear model was reported to be in error by as much as 6.5%. The largest errors occurred in the region where Mode II was dominant. These results showed that the current ASTM standard which does not include corrections for nonlinear errors could produce data which is significantly in error when testing very tough composites. This problem is expected to become worse as even tougher composites are developed.

The model used by Sainath[*9*] only corrects for crack length shortening due to opening displacement. In the current paper 5 different data reduction schemes for the MMB test are presented. One of these schemes uses a new iterative nonlinear analysis which accounts for all of the sources of error identified in Figure 3. An example problem is then used to highlight differences between the 5 data reduction schemes. The iterative nonlinear model, which is assumed to be the most accurate, is then used to formulate a criterion which limits the nonlinear error to a small value so that a linear model can be used.

Analyses of the MMB Test

Five different data reduction schemes are compared in this paper. The linear model (LN) will be used as the baseline because it is the basis for the data reduction scheme that is called for in the ASTM standard. The basic beam theory model (BT) is also a linear model derived from Euler-Bernuli beam theory but without correction terms that are found in the LN model. This model will be used to help explain some of the characteristics of the nonlinear models. The iterative nonlinear model (NL) accounts for all four of the sources of nonlinear error identified in Figure 3, and therefore, it is believed to be the most accurate of the 5 models presented. The Kinloch model (KIN) is a nonlinear model that accounts for crack length shortening shown in Figure 3a. Finally, the modified Kinloch model (MK) corrects the KIN model for some deficiencies that will be described in the paper. Figure 4 shows many of the model parameters which will be used in the following sections.

Linear Model (LN)

The linear model is used to derive the equations used in the ASTM standard and is the basis against which the others will be compared. The equations are based on basic beam theory but are adjusted for deformation near the crack tip that causes the displacements (and G) to be larger than that predicted from basic beam theory. The corrections proposed by Williams[*11*] are based on a curve fit to FEM results where the

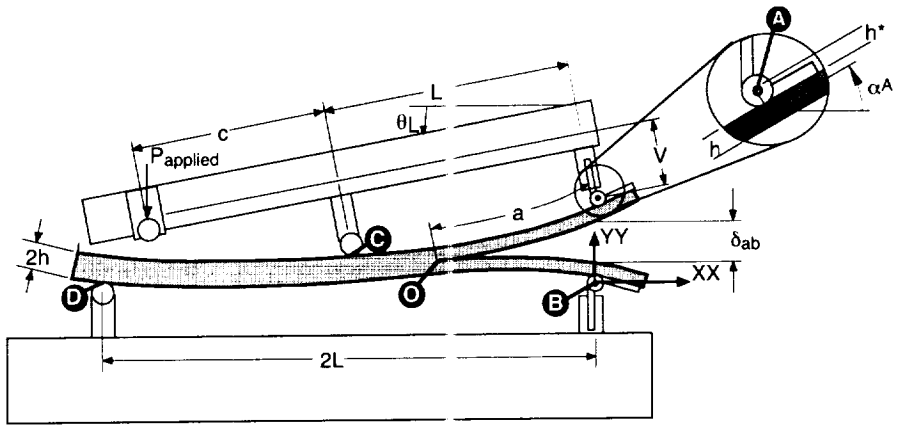

Figure 4—*Diagram of MMB apparatus showing model parameters.*

magnitude of the deformation of a Mode I specimen corresponds to a specimen with the crack length artificially increased by χh. The χ parameter is a function of the in-plane and the out-of-plane elastic moduli of the graphite composite material, and h is the half thickness of the specimen. The correction to the Mode II deformation was found to be similar but the effective increase in crack length was found to be $0.42\chi h$ [*12*]. The η_I and η_{II} parameters (defined under parameter definitions in the nomenclature section) are used to scale the Mode I and Mode II deformations to account for the corrected crack lengths. The following equations were used to calculate displacements, rotations, and strain energy release rate values:

$$\delta = \frac{P_{applied}}{96EI}\left[64\left(\frac{3c-L}{4L}\right)^2 a^3\eta_I + \left(\frac{c+L}{L}\right)^2\left(2L^3+3a^3\right)\eta_{II}\right] \tag{1}$$

$$\delta_{ab} = \frac{2P_{applied}}{3EI}\left[\left(\frac{3c-L}{4L}\right)a^3\eta_I\right] \tag{2}$$

$$\alpha^A = \frac{P_{applied}}{32EI}\left[\frac{16}{3}\left(\frac{3c-L}{4L}\right)\left(\frac{a+3L}{L}\right)a^2\eta_I + \left(\frac{c+L}{L}\right)\left(\frac{L^3+3a^2L-a^3}{L}\right)\eta_{II}\right] \tag{3}$$

$$\alpha^B = \frac{P_{applied}}{32EI}\left[\frac{16}{3}\left(\frac{3c-L}{4L}\right)\left(\frac{a-3L}{L}\right)a^2\eta_I + \left(\frac{c+L}{L}\right)\left(\frac{L^3+3a^2L-a^3}{L}\right)\eta_{II}\right] \tag{4}$$

$$\alpha^O = \frac{P_{applied}}{32EI}\left[\frac{16}{3}\left(\frac{3c-L}{4L}\right)\left(\frac{a^3}{L}\right)\eta_I - \left(\frac{c+L}{L}\right)\left(\frac{L^3-a^2L-a^3}{L}\right)\eta_{II}\right] \tag{5}$$

$$G_I = \frac{P_{applied}^2}{b\,EI}\left(\frac{3c-L}{4L}\right)^2 (a+\chi h)^2 \qquad G_{II} = \frac{3P_{applied}^2}{64\,b\,EI}\left(\frac{c+L}{L}\right)^2 (a+0.42\chi h)^2 \qquad (6)$$

Basic Beam Theory Model(BT)

The most basic model of the MMB specimen based on Euler-Bernuli beam theory. Results from basic beam theory are created by using the linear model equations but with χ set to 0. (η_I and η_{II} therefore become 1)

Iterative Nonlinear Model (NL)

The linear model predicts deformations based on the loading applied to the specimen. The deformations change the loading on the specimen so the nonlinear model iterates until a deformation is obtained which is consistent with the loading that created it. The model uses a local coordinate system defined by the crack tip to describe displacements. The choice of coordinate system reduces rotations that can cause nonlinear error. The equations used in the NL model start with the basic beam theory equation. The deformations are separated into Mode I and Mode II components so that they can be scaled by the appropriate factor using the Williams χ corrections[*11*]. Once a converged deformed shape is obtained, a second correction is made to account for the shortening of the crack length due to large bending deformations. This is based on a formulation which was also proposed by Williams[*11*]. The nonlinear model is similar to the nonlinear model used when the mixed-mode bending fixture was redesigned to minimize nonlinear errors[*6*] but differs in the treatment of deformation about the crack tip. The iterative nonlinear model found in reference [*6*] also did not include the crack shortening correction which has been added to the current model. The iterative nonlinear model is given in the Appendix.

Kinloch Model (KIN)

The Kinloch model[*10*] uses the correction proposed by Williams[*11*] to correct for the shortening crack length. Other sources of nonlinear error are not considered. The implementation of this correction calls for the measurement of the Mode I opening (δ_{ab}) during the MMB test (Figure 4). This opening displacement is then used to predict the rotation of the crack tip and rotation of the specimen at each hinge. These rotations are used to predict the shortening of the crack length due to the large beam deformations. The shortening of the crack length causes the loading at the crack tip to change, and therefore, the value of G_T also changes. To correct the toughness value, the moments on the upper and lower arms are scaled (F_a and F_b, respectively) to correct for shortening of the lever arm. In this paper, the δ_{ab} input into the model was taken from the NL model.

The following model is presented from Kinloch et al.[*10*] and is presented in exactly the same form as the original except that the notation was modified to be consistent with the rest of the notation in this paper. This includes substituting 2L for the full span length and L for the distance between the center roller to the hinge. These were originally distinct values since the derivation was for an apparatus with an unsymmetrical span length.

$$\xi = \frac{16a^3}{3\delta_{ab}}(q-m) \quad \text{where} \quad m \equiv \frac{1-\frac{L+c}{2L}}{\left(1+\frac{c}{L}\right)\left(1-\frac{L}{2L}\right)} \qquad q \equiv \frac{\frac{c}{L}}{\left(1+\frac{c}{L}\right)\left(1-\frac{L}{2L}\right)} \qquad n \equiv \frac{L}{2L-L} \quad (7)$$

$$\alpha^O = \frac{2}{3(2L)\xi}\left[n(2L-L)^3 + a^3(1-8m)\right] + \frac{L^2-a^2}{\xi} \quad (8)$$

$$\alpha^A = \alpha^O + \frac{8qa^2}{\xi} \quad (9)$$

$$\alpha^B = \alpha^O + \frac{3ma^2}{\xi} \quad (10)$$

$$F_a = 1 - \frac{3(\alpha^O)^2 + 4\alpha^O\alpha^A + 8(\alpha^A)^2}{30} \quad (11)$$

$$F_b = 1 - \frac{3(\alpha^O)^2 + 4\alpha^O\alpha^B + 8(\alpha^B)^2}{30} \quad (12)$$

$$G_I = \frac{3P^2_{\text{applied}}(a+\chi h)^2}{b^2 E_{11} h^3}\left[\left(1-\frac{c+L}{2L}\right)F_b - \left(\frac{c}{L}\right)F_a\right]^2 = \frac{P^2_{\text{applied}}}{4b^2 EI}\left[\frac{2(L-c)F_b - 4cF_a}{4L}\right]^2 (a+\chi h)^2 \quad (13)$$

$$G_{II} = \frac{9P^2_{\text{applied}}(a+0.42\chi h)^2}{4b^2 E_{11} h^3}\left[\left(1-\frac{c+L}{2L}\right)F_b + \left(\frac{c}{L}\right)F_a\right]^2 = \frac{3P^2_{\text{applied}}}{64b^2 EI}\left[\frac{(L-c)F_b + 2cF_a}{L}\right]^2 (a+0.42\chi h)^2 \quad (14)$$

Modified Kinloch Model (MK)

One more model will be developed based on the Kinloch model[*10*] but modified as suggested by results from the example problem presented in the next section. Equations 15-18 are substituted for equations 7-10 in the previous model, respectively. The changes to the previous equations are clearly marked. The addition of the L^3 term in equation 16 is the inclusion of a term that had inadvertently been dropped in the original

derivation. The other changes involve the η and η_{II} parameters which more accurately partition the Mode I and Mode II components of deformation.

$$\xi = \frac{16a^3}{3\delta_{ab}}(q - n)\overbrace{\frac{\eta_I}{\eta_{II}}}^{\text{change}} \tag{15}$$

$$\alpha^O = \frac{2}{3(2L)\xi}\left[n(2L-L)^3 \overbrace{-L^3}^{\text{change}} + a^3(\quad - 8\overbrace{(\frac{1}{2} - \frac{(q-m)}{2}\frac{\eta_I}{\eta_{II}})}^{\text{change}}\right] + \frac{L^2 + a^2}{\xi} \tag{16}$$

$$\alpha^A = \alpha^O + \frac{8a^2}{\xi}\overbrace{(\frac{1}{2} + \frac{(q-m)}{2}\frac{\eta_I}{\eta_{II}})}^{\text{change}} \tag{17}$$

$$\alpha^B = \alpha^O + \frac{8a^2}{\xi}\overbrace{(\frac{1}{2} - \frac{(q-m)}{2}\frac{\eta_I}{\eta_{II}})}^{\text{change}} \tag{18}$$

Comparison of Data Reduction Models Using a Numerical Example Problem

To first explore these models the test case presented by Sainath[9] will be investigated. The numerical values to be used in the example problem are given in Table 1. Notice that the value of V and h* were not given in the original paper and so typical values were chosen. The toughness results calculated from the linear (LN), nonlinear (NL) and Kinloch (Kin) models are shown in Table 2. Both G_T and G_{II}/G_T are calculated for each method. The percent deviation form the linear model is also calculated for each nonlinear prediction. The deviation from the linear model can be thought of as the predicted error caused by ignoring the nonlinear effects. In all cases, the prediction of G_T by the KIN model is smaller than the linear model while the prediction of the NL model is larger than the linear. Also, the magnitude of the deviation predicted by the KIN model is generally twice as great as that from the NL model. Note that a prediction at 100% G_{II}/G_T cannot be made with the KIN model because it uses a Mode I displacement as input which goes to 0 at 100% G_{II}/G_T.

Table 1—*Example numerical values*

Parameter	Value
E_{11}	142 GPa (20.6 Msi)
E_{22}	10.5 GPa (1.53 Msi)
G_{12}	4.1 GPa (0.6 Msi)
L	51 mm (2.00 in)
a	25.5 mm (1.004 in.)
b	25.48 mm (1.003 in)
h	1.5 mm (0.057 in)
h*	2.5 mm (0.1 in)
V	15 mm (0.6 in)

Table 2—*Toughness results from nonlinear models*

G_{II}/G_T %	c mm	$P_{applied}$ N	G_T kJ/m^2				G_{II}/G_T %			
			LN	NL	KIN	MK	LN	NL	KIN	MK
40	48.6	334	1.27	1.29	1.23	1.25	41.9	40.1	41.9	41.9
Deviation	--	--	--	**1.9%**	**-3.5%**	**-1.8%**	--	**-2.1%**	**0.1%**	**0.0%**
60	36.3	504	1.55	1.60	1.48	1.50	59.7	56.9	60.0	59.9
Deviation	--	--	--	**3.0%**	**-5.5%**	**-2.5%**	--	**-2.8%**	**0.6%**	**0.4%**
80	27.1	727	2.05	2.13	1.79	1.82	81.0	78.9	81.1	81.1
Deviation	--	--	--	**3.7%**	**-8.2%**	**-3.3%**	--	**-2.1%**	**0.1%**	**0.1%**
100	16.8	1213	3.25	3.30	--	--	100.0	99.5	--	--
Deviation	--	--	--	**1.5%**	--	--	--	**-0.5%**	--	--

To understand why the predictions of the KIN and NL models are so different the predicted displacements were examined. Table 3 shows three different displacements: 1) δ_{ab}, the vertical displacement between the hinges which is associated with a Mode I deformation; 2) $\alpha_I = (\alpha^A - \alpha^B)/2$, the difference in slope between the top and bottom hinge, which corresponds to the angle if the entire loading were in Mode I; and 3) $\alpha_{II} = (\alpha^A + \alpha^B)/2$, the average of the top and bottom slope at the hinges, which is dominated by the Mode II deformation[†]. The displacements are shown for the linear (LN), beam theory (BT), nonlinear (NL), and Kinloch (KIN) models. The deviations from the LN model are also calculated and displayed in the table.

Comparison of the deformation values shows that BT model significantly under predicts (-30%) the Mode I deformation from the LN model while agreeing on the Mode II deformation reasonably well. The NL model is believed to provide the most accurate prediction of deformation and the results show there is little difference between the NL and LN model predictions of deformation. The one exception is that when the Mode I component was small, the deviation in Mode I displacement could become significant (13% and larger). The KIN model agrees with the LN model (and therefore the NL model) in the Mode I deformation but shows very significant deviation on the Mode II prediction (64-86%). Two reasons were found for this discrepancy in Mode II. First, in the original derivation of the KIN model[*10*], the equation used to describe the rotation at the crack tip (α^O) which was derived using basic beam theory was found to have a missing term. Equation 16 shows how this L^3 term is added into the equation for α^O. Second, the KIN model uses the measured value of δ_{ab} to predict the slope of points A, B, and O on the specimen based on basic beam theory. Because basic beam theory grossly under-predicts Mode I deformation, when the Mode I deformation (δ_{ab}) is used as input, the resulting predictions of the Mode II deformation (such as $\alpha_{II} = (\alpha^A + \alpha^B)/2$) is largely over-predicted. The large over prediction of the Mode II deformation pattern caused the predicted error in G_T to be worse than is actually the case.

The two previously discussed problems with the KIN model were fixed in the Modified Kinloch model (MK). In this model the missing term in the α^O equation is added and deformations are predicted using the χ crack length correction terms which

---

[†] α_{II} is not completely mode II because of a contribution made by a rigid body rotation of the mode I deformed body required to keep the far end of the specimen on the roller at point D.

Table 3—*Displacement results from nonlinear models*

G_I/G_{II} %	δ_{ab} mm			$\alpha_I = (\alpha^A - \alpha^I)/2$					$\alpha_{II} = (\alpha^A + \alpha^B)/2$				
	LN	BT	NL	LN	BT	NL	KIN	MK	LN	BT	NL	KIN	MK
40	2.21	1.55	2.29	0.068	.048	0.071	0.070	0.070	0.098	0.092	0.100	0.161	0.101
Deviation	--	**-30%**	**3%**	--	**-30%**	**5%**	**3%**	**3%**	--	**-6%**	**2%**	**64%**	**3%**
60	2.06	1.45	2.18	0.062	0.044	0.068	0.066	0.066	0.124	0.119	0.127	0.214	0.132
Deviation	--	**-30%**	**6%**	--	**-30%**	**8%**	**6%**	**6%**	--	**-4%**	**2%**	**73%**	**6%**
80	1.56	1.09	1.78	0.047	0.043	0.055	0.054	0.054	0.155	0.150	0.159	0.289	0.176
Deviation	--	**-29%**	**13%**	--	**-30%**	**16%**	**13%**	**13%**	--	**-3%**	**3%**	**86%**	**14%**
100	0	0	0.38	0.000	0.000	0.0128	0.0116	0.0116	0.214	0.209	0.221	Large	Large
Deviation	--	**0%**	**Large**	--	**0%**	**Large**	**Large**	**Large**	--	**-2%**	**3%**	**Large**	**Large**

were used in the LN model. Table 3 shows that the MK model does a reasonably good job of predicting both the Mode I and Mode II deformations. Table 2 also shows that these modifications to the KIN model cause the predicted deviation from the LN model to be cut by half in this test case. The MK model predicts the error caused by ignoring the nonlinear effect on G_T to be less than 4% in all cases.

Several problems remain with the MK model. First, it only models the nonlinear problem of crack length shortening due to beam deformation. There are several other sources of nonlinear error. Since in this test case the MK model always predicted a negative deviation in G_T while the NL model always predicted a positive deviation, the phenomenon modeled by the MK model does not even appear to be the dominant effect. A second problem with the MK model is that it is based on a measured Mode I displacement, which causes problems in the high Mode II region. To a first order approximation at a given mixed-mode condition, the correction to G_T (LN) predicted by the MK model can be shown to be proportional to the measured value of δ_{ab} squared (Correction Factor =Constant $(\delta_{ab})^2$). When G_{II}/G_T approaches 1, δ_{ab} approaches 0. This might not cause a problem if the error in G_I also went to zero but the error in G_T can remain large, so the constant value must become very large. Under this condition small errors in the measured δ_{ab} can produce large errors in the MK model predictions of G_T. Finally at $G_{II}/G_T=1$, δ_{ab} =0 and the correction cannot be used even though the error due to the shortening crack length remains. This makes the Mode II value inconsistent with the other calculations of toughness. A third drawback to using the MK correction is that it requires that an extra measurement be made during the test. Each extra measurement adds complexity to the test method. For the preceding reasons neither the KIN nor the MK corrections are recommended when analyzing MMB test results.

The NL model is believed to provide a better estimate of the nonlinear problems, but it is too complicated to be of general use in determining delamination toughness. Fortunately the nonlinear problem does not seem to be as significant as first thought based results that were generated using the KIN model. In time however, materials that are so tough that nonlinear errors do become significant may be developed. Currently available materials tested with a poorly designed test specimen (i.e. one that is too compliant) could also result in toughness values that contained significant errors. Because of this, some way of avoiding the nonlinear errors without requiring an analysis such as the NL model is needed.

A New Nonlinear Error Avoidance Criterion

One method to avoid nonlinear errors would be to develop correction factors predicted using the NL model which have been plotted based on a few critical parameters. Unfortunately the nonlinear errors in this problem are influence by a large number of parameters. The most significant influences seem to come from the following parameters:

Normalized lever position therefore mixed-mode ratio ($c/L \rightarrow G_{II}/G_T$)
Applied load and therefore toughness ($P_{applied} \rightarrow G_T$)
Specimen stiffness (EI)
Normalized crack length (a/L)
Span length (L)
Normalized hinge height (h*/L)
Normalized lever loading height (V/L)

Each of these parameters affects one or more of the sources of nonlinear error shown in Figure 3 and the effect of each of these parameters is shown in Figure 5. In Figure 5, the error in a G_T value calculated using the LN model is plotted versus G_{II}/G_T, which is varied by varying the normalized lever length (c/L). For each of the other parameters, a nominal value is chosen at a level similar to that studied in the example problem. Each parameter was then varied to values above and below the nominal value. The range of bending stiffness (EI) was attained by keeping modulus at 138 GPa (20 Msi) and letting h take on the values of 1.1, 1.5, and 2.2 mm (0.045, 0.06 and 0.085 in. respectively) with 1.5 mm (0.06 in.) being the nominal value. In Figure 5, the first plot shows the error with all parameters at their nominal value and also with all possible variations. This plot shows that the nonlinear error in the nominal case is quite small, but when all the possible variations are considered, the error can become quite large (much greater than 10%).

To understand how the large errors were produced, each parameter was considered individually. A plot was made with each parameter showing how varying just the one parameter above and below the nominal value effected the nonlinear error. On each of these plots, the possible errors produced by holding the one parameter at the nominal value while changing all the others was also shown. From these plots, it is clear that, with the exception of the small bending stiffness case, no one variation from the nominal creates an overriding amount of error. It can also be seen that the error can remain quite large if only one parameter is tightly controlled. The variations in the shapes of the error curves and the fact that the values are positive and negative indicates that the variables are interacting in complex, often compensating ways and no simple way of estimating the error based on these variables was found

A simple way of avoiding large errors due to nonlinear deformation, however, was found. Although each parameter effects the error directly and interacts with the other parameters to effect the error indirectly, the error in all cases is due to the deformation of the test specimen. Figure 6 shows values of normalized applied displacement (δ/L) required to exceed a nonlinear error of -5%. Here the applied load and therefore G_T is varied to achieve the deformation, and one parameter, the V/L value, is constrained at the nominal value (0.3). All other variables are varied over the range already given in

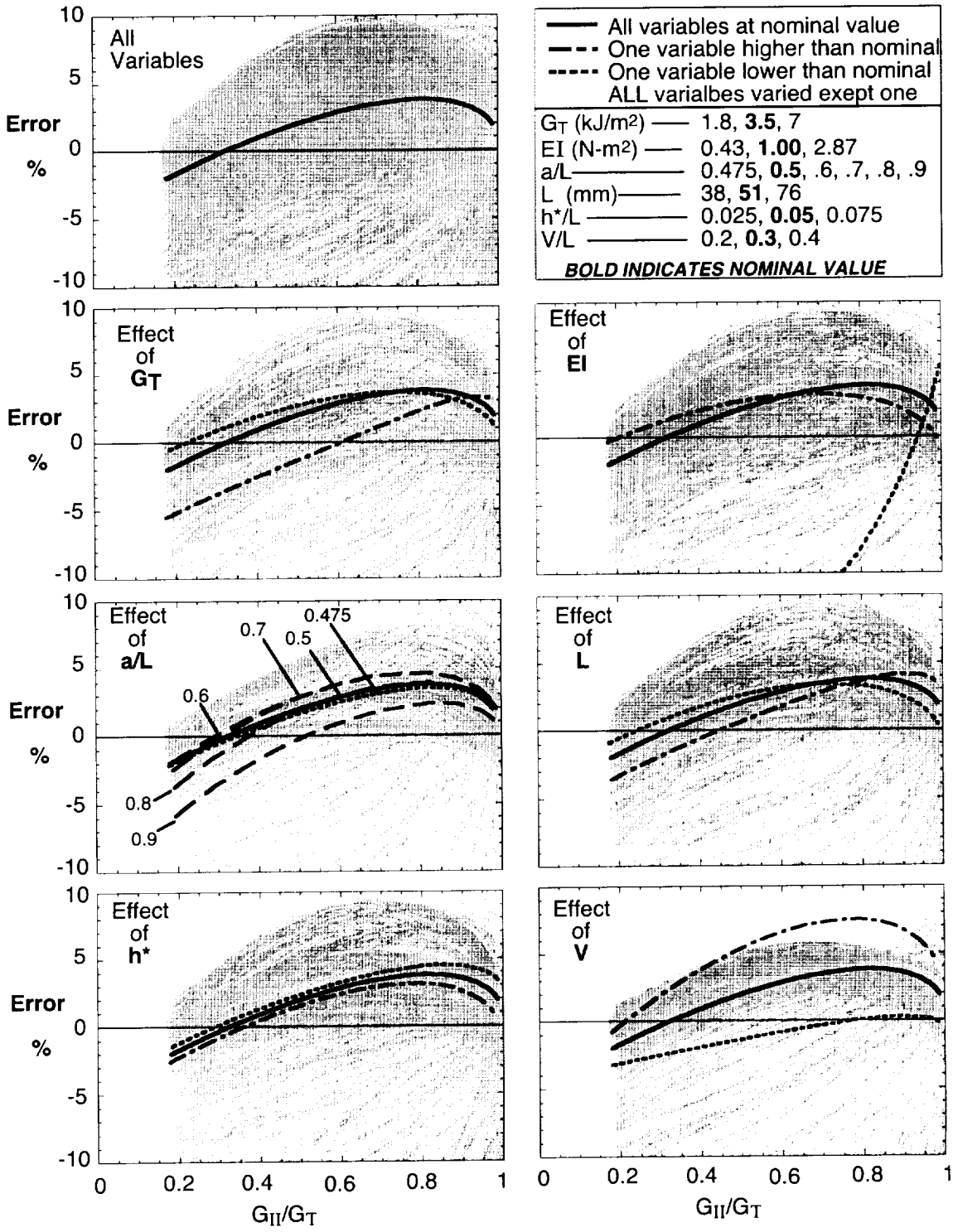

Figure 5—*Effect of test parameters on nonlinear error*

Figure 5. From this plot, it is clear that the curves are greatly consolidated, and it is possible to define a lower bound where the |error| will not be greater than 5%. If the nonlinear error is less than 5%, then in a linear problem the predicted load for delamination growth would only be off by 2 5%. This error is small enough that it can normally be considered negligible. This nonlinear error avoidance criterion is:

$$\delta/L < 0.27 - 0.06\, G_{II}/G_T \tag{19}$$

The nonlinear avoidance criterion is valid over the entire range of mixed-mode ratios and crack lengths over which the MMB test can be conducted ($0.2 < G_{II}/G_T < 1.0$, $0.475 < a/L < 0.9$) but requires that the load point height be set to V/L= 0.3. The criterion is sensitive to hinge height so the hinge height should not be greater the range studied here ($h^*/L < 0.075$). The bending stiffness (EI) and the half span length (L) were both varied over a wide range so their values are not believed to be as critical.

Figure 7 shows the values of toughness that are attained using the nonlinear error avoidance criterion. This shows that the test parameters, which are chosen have an overriding influence on the toughness values that can be attained before the nonlinear error avoidance criterion is violated. It also shows that the toughness values that can be attained in the high Mode I region is much less than that which can be attained in the high Mode II region. Because Mode I toughness is rarely more than 0.9 kJ/m^2 (5 in-lb/in^2) while Mode II fracture toughness can be four times that amount, the lower values of toughness attainable in the high Mode I region will normally not be a problem. The high values of toughness attainable with the nominal test parameters indicates that by

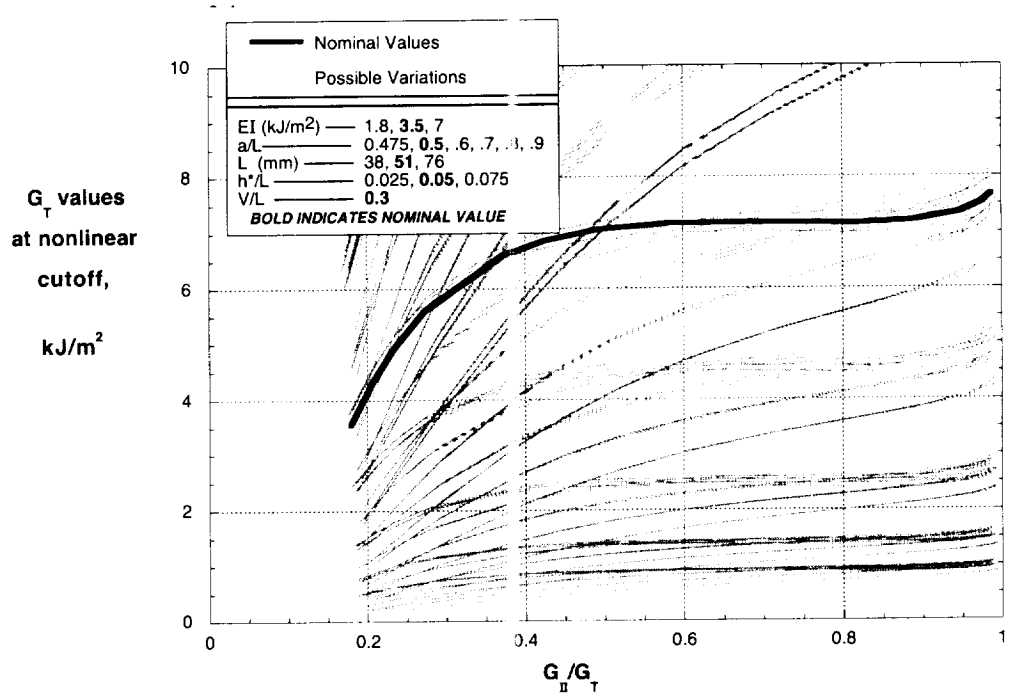

Figure 7—*Toughness values attainable while avoiding large nonlinear errors*

picking reasonable specimen parameters, the toughness of extraordinarily tough materials can be measured. On the other hand by picking the test parameters poorly, the cutoff displacement for nonlinear error would be reached before attaining the critical toughness for even moderately tough materials. The linear equation for MMB deformation given as equation 20 can be used to predict when the displacement will become large enough to violate the nonlinear error avoidance criterion and can also be used as a guide for choosing test parameters where nonlinear errors will not be significant. Generally by keeping the specimen thickness in the nominal range or higher and by not making the specimen length (L) higher than normal, the error due to nonlinearity will not be a problem.

$$\delta_{cst} = \frac{P_{cst}}{8\, b\, E_{11}\, h^3\, L^2}\left[4(3c-L)^2(a+h\chi)^3 + (c+L)^2\left(2L^3 + 3(a+0.42h\chi)^3\right)\right] \tag{20}$$

where

$$P_{cst} = \sqrt{\frac{\frac{4}{3} G_T \, b^2 E_{11}\, h^3 L^2}{(3c-L)^2(a+h\chi)^2 - \frac{3}{4}(c+L)^2(a+0.42h\chi)^2}} \tag{21}$$

It is possible that the mixed-mode ratio could be significantly in error even though the error in G_T is small. As a final check, Figure 8 shows the error in G_{II}/G_T when the

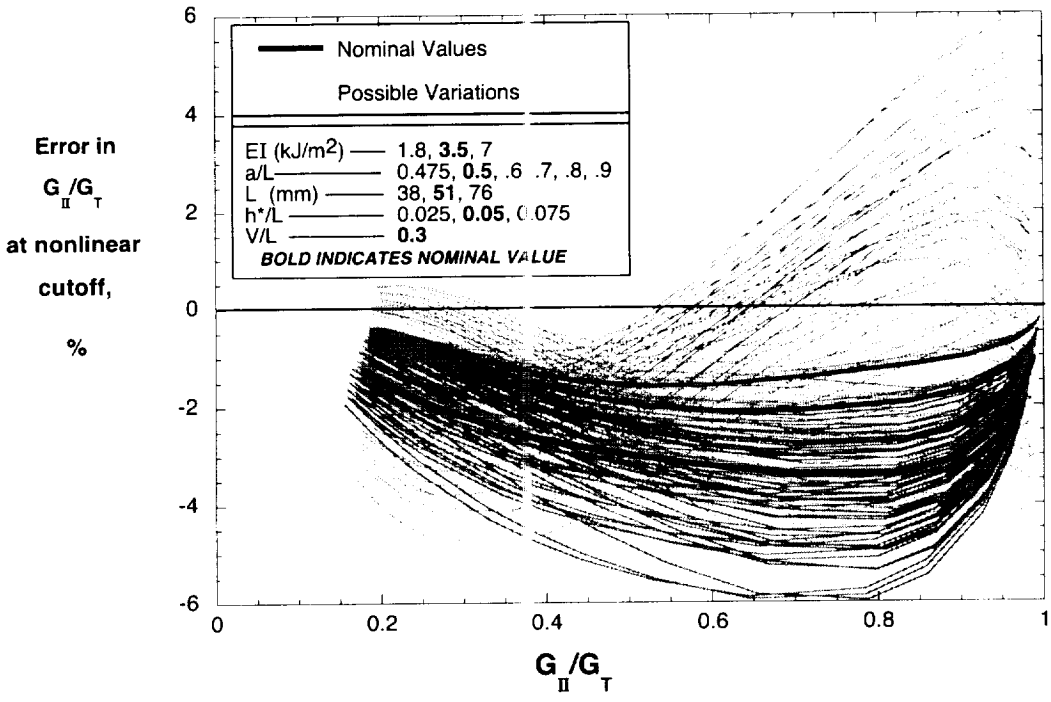

Figure 8—*Error in G ratio at nonlinear error avoidance criterion*

loading on the MMB test reaches the nonlinear error avoidance criterion. It is clear that, in all cases studied, the applied displacement criterion also restrains the error in mixed-mode ratio to a small value. In all but a few extreme cases, the deviation from the linear values is less than 5%. The nonlinear avoidance criterion can therefore be used to limit the use of the MMB test to conditions where the linear model accurately calculates both the G_T and the G_{II}/G_T values.

Conclusions

The new test standard for mixed-mode delamination toughness (ASTM D 6671-01) had previously been shown to incur significant errors due to geometric nonlinearity when testing very tough materials. A nonlinear model was created that modeled several sources of geometric nonlinear error. The magnitude of these errors was shown to be significantly less than had previously been reported, but with very tough materials or with very compliant test specimen, nonlinear errors could become significant. The magnitude of the nonlinear error was shown to be a complicated function of many test parameters, including: material toughness, the mixed-mode ratio, the specimen bending stiffness, the specimen length, the height of the loading hinge, and the height of applied load. A very simple nonlinear error avoidance criterion was developed based on the magnitude of the displacement at the applied load. All the test parameters were allowed to vary over a significant range except for the height of the applied load, which was set at $V/L = 0.3$ above the hinge attachment point, and the height of the hinge is less than $h^*/L < 0.075$. The nonlinear error should generally not be a problem, but equations are presented which can be used to redesign a test specimen where the applied displacement become large enough to violate the nonlinear error avoidance criterion."

References

[1] Russell, A. J., "On the Measurement of Mode II Interlaminar Fracture Energies," Defense Research Establishment, Victoria December 1982.

[2] Kenane, M. and Benzeggagh, M. L., "Mixed-mode delamination fracture toughness of unidirectional glass/epoxy composites under fatigue loading," *Composites Science and Technology*, vol. 57, pp. 597-605, 1997.

[3] Sriram, P., Khourchid Y., Hooper, S. J., and Martin, R. H., "Experimental Development of a Mixed-Mode Fatigue Delamination Criterion," in *Composite Materials: Fatigue and Fracture*, vol. 5, 1995, pp. 3-18.

[4] Liu, Z., Gibson, R. F., and Newaz G. M , "Modification of the Composite Laminate Mixed Mode Bending Test for Fracture Testing of Adhesive Joints," presented at The American Society for Composites, 5th Technical Conference, College Station, 2000.

[5] Reeder, J. R. and Crews, J. H., Jr. , "Mixed-Mode Bending Method for Delamination Testing," *AIAA Journal*, vol. 28, pp. 1270-1276, 1990.

[6] Reeder, J. R. and Crews, J. H., Jr., "Nonlinear Analysis and Redesign of the Mixed-Mode Bending Delamination Test,",, *NASA TM-102777*, 1991.

[7] Reeder, J. R. and Crews, J. H. Jr., 'Redesign of the Mixed-Mode Bending Delamination Test to Reduce Nonlinear Effects," *Journal of Composites Technology & Research ISSN 0885-6804 Journal of Composites Technology & Research (ISSN 0885-6804), vol. 14, no. 1, Spring 1992, p. 12-19.*, 1992.

[8] Shivakumar, K. N., Crews, J. H., Jr. and Avva, V. S., "Modified Mixed-Mode Bending Test Apparatus for Measuring Delamination Fracture Toughness of Laminated Composites," *Journal of Composite Materials*, vol. 32, pp. 804-828, 1998.

[9] Sainath, S., "Verification of a Non-Classical Energy Release Rate Based Approach For Predicting Delamination Growth in a Two-Phase Graphite/Epoxy Composite Material," Master's Thesis in the Department of Mechanical, Aerospace and Manufacturing Engineering: Syracuse University, 1999.

[10] Kinloch, A. J., Wang, Y., Williams J. G. and Yayla, P., "The Mixed-Mode Delamination of Fibre Composite Materials," *Composites Science and Technology*, vol. 47, 1993, pp. 225-237.

[11 Williams, J. G., "The Fracture Mechanics of Delamination Tests," *Journal of Strain Analysis for Engineering Design*, vol 24, 1989, pp. 207-214.

[12] Wang, Y. and Williams, J. G., "Corrections for Mode II Fracture Toughness Specimens of Composite Materials,' *Composites Science and Technology*, vol. 43, 1992, pp.251-256.

[13] Kanninen, M. F., "An Augmented Double Cantilever Beam Model for Studying Crack Propagation and Arrest," *International Journal of Fracture*, vol. 9, no. 1, March 1973, pp.83-92.

[14] Aliyu, A. A. and Daniel, I. M. "Effects of Strain Rate on Delamination Fracture Toughness of Graphite/Epoxy," in *Delamination and Debonding of Materials, ASTM STP 876*, W. S. Johnson, Ed., American Society for Testing and Materials, West Conshohocken, PA, 1985, pp. 336-348.

[14] Carlsson, L. A. and Gillespie, F. W., "On The Analysis and Design of the End Notch Flexure (ENF) Specimen for Mode II Testing," *Journal of Composite Materials*, vol. 20, 1986, pp. 594-604.

[16] Bhashyan, S. and Davidson, B. D., "An Evaluation of Data Reduction Methods for the Mixed Mode Bending Test," in the proceedings of the 37th Structures, Structural Dynamics and Materials Conference, Salt Lake City, UT, 1996, pp. 886-896.

Appendix Nonlinear Iterative Model (NL)

The nonlinear model is similar to the model presented by Reeder and Crews[*6*] with a couple of significant changes:

1. The deformation equations derived from beam theory must be corrected for shear deflection and for rotations that occur around the crack tip. In the original model, corrections based on a beam on elastic foundation analysis[*13*] and including shear deformation[*14,15*] were used. In the current model, corrections originally suggested by Williams[*11,12*] employing the χ crack length correction terms which are based on a curve fit to finite element results. These Williams corrections are used because they have been shown to be more accurate[*16*] and to be consistent with the equations from the ASTM standard which uses the χ parameters. Since these corrections were formulated for the Mode I and Mode II tests, to apply them to the MMB test, the deformation had to be divided into a Mode I and Mode II component.
2. The nonlinear correction for the crack length shortening suggested by Williams[*11*] was included in the current analysis.

It was convenient to use two different coordinate systems in this model as shown in Figure A1. The origin of the first is located at the crack tip and is termed the specimen coordinate system. Positions in this coordinate system are signified by X and Y, and parameters expressed in this coordinate system are indicated by a superscript X or Y. The term ϕ is used to refer to the slope of the specimen in the specimen coordinate system. Superscripts of A, B, C, D, or O refer to the position on the specimen. The origin of the second coordinate system is at point B with a reference angle parallel to the base of the apparatus. This coordinate system is termed the global coordinate system because it corresponds to the frame of reference that would normally be observed in testing. Note that θ_o is the angle between the two coordinate systems.

Step 1. Initial position and loading of specimen

The following load values were used to initiate the iterative analysis. These equations can be obtained from summing forces and moments on the lever and the specimen before any deformation occurs. Note that initially the two coordinate systems will be identical except for a shift in origin from point O to point B.

$$P_Y^A = P_{applied}\frac{c}{L} \qquad P_Y^B = P_{applied}\frac{L-c}{2L}$$

$$P_Y^C = -P_{applied}\frac{c+L}{L} \qquad P_Y^D = -P_{applied}\frac{L+c}{2L}$$

$$P_I = P_{applied}\frac{3c-L}{4L} \qquad P_{II} = P_{applied}\frac{L+c}{L}$$

$$P_X^A = P_X^B = P_X^C = P_X^D = 0$$

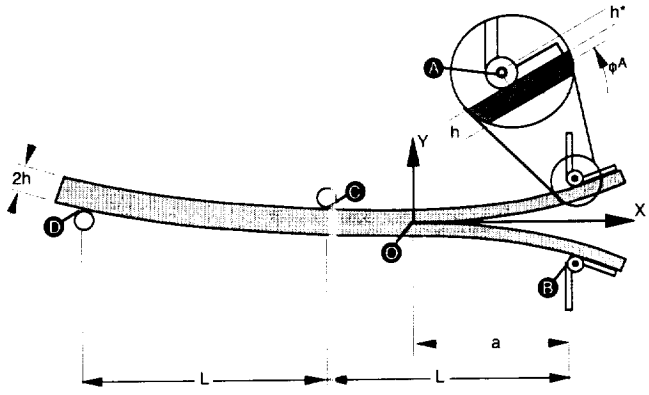

a) Specimen coordinate system

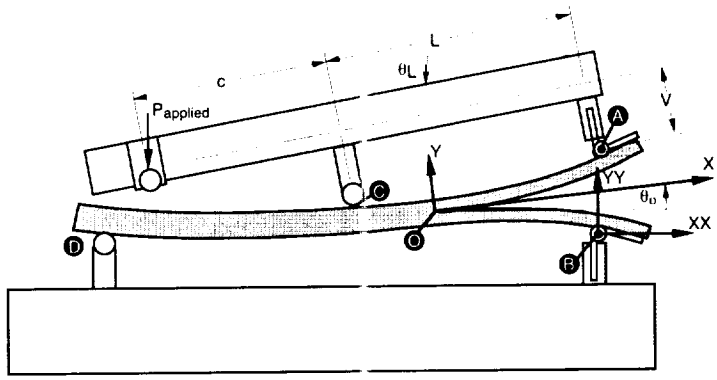

b) Global coordinate system

Figure A1. *Model coordinate systems and notation.*

Step 2. Calculation of specimen position based on specimen loading.

The position and slope of each point on the specimen must be calculated to determine how the loading changes with deformation. The terms involving ϕ^A and ϕ^B account for the shortening of the crack length due to hinge rotation as shown in Figure 2c. The calculation of Y displacement and rotation (ϕ) are all calculated based on the deformation that would occur due to the Mode I and Mode II deformation. Each mode of deformation is scaled by a correction term (η_I and η_{II}, respectively) derived from the χ correction term used to calculate strain energy release rate. All deformations at points C and D are assumed to be associated with Mode II.

$$X^A = a - \phi^A\left(\frac{h}{2} + h^*\right) \qquad Y^A = \frac{P_I a^3}{3EI}\eta_I + \frac{P_{II} a^3}{12EI}\eta_{II} + h + h^*$$

$$\phi^A = \frac{P_I a^2}{2EI}\eta_I + \frac{P_{II} a^2}{8EI}\eta_{II}$$

$$X^B = a - \phi^B\left(\frac{h}{2} + h^*\right) \qquad Y^B = -\frac{P_I a^3}{3EI}\eta_I + \frac{P_{II} a^3}{12EI}\eta_{II} - h - h^*$$

$$\phi^B = -\frac{P_I a^2}{2EI}\eta_I + \frac{P_{II} a^2}{8EI}\eta_{II}$$

$$X^C = a - L \qquad Y^C = \left(\frac{P_Y^C (L-a)^3}{24EI} + \frac{P_Y^D (L-a)^2 (5L-2a)}{48EI}\right)\eta_{II} + h$$

$$\phi^C = -\left(\frac{P_Y^C (L-a)^2}{16EI} + \frac{P_Y^D (L-a)(3L-a)}{16EI}\right)\eta_{II}$$

$$X^D = a - 2L \qquad Y^D = \left(\frac{P_Y^C (L-a)^2 (5L-2a)}{48EI} + \frac{P_Y^D (2L-a)^3}{24EI}\right)\eta_{II} - h$$

$$\phi^D = -\left(\frac{P_Y^C (L-a)^2}{16EI} + \frac{P_Y^D (2L-a)^2}{16EI}\right)\eta_{II}$$

Step 3. Calculation of global position based on deformed specimen.
To determine the location of the specimen in the global coordinate system the following equations are used. The angle between the local coordinate system and the global system is obtained for the vertical displacement between the base hinge support and the right roller support divided by the horizontal distance. A similar approach is used to determine the angle of the MMB lever. The global position of point O is determined by a simple transfer in the coordinate system.

$$\theta_o = -\mathrm{Tan}^{-1}\left[\frac{Y^B - Y^D + h^*}{2L}\right] \qquad \theta_l = \theta_o + \mathrm{Tan}^{-1}\left[\frac{Y^A - Y^C - h^*}{L}\right]$$

$$XX^o = -X^B \mathrm{Cos}[\theta_o] + Y^B \mathrm{Sin}[\theta_o] \qquad YY^o = -X^B \mathrm{Sin}[\theta_o] - Y^B \mathrm{Cos}[\theta_o]$$

Step 4 Calculation of specimen loading based on deformed shape.

The loading on the specimen begins by translating the applied load, which is vertical in the global coordinate system, into the specimen coordinate system. The rest of the loading is determined by the summing the loads and moments on the lever to determine the loading at A and C and then on the specimen to determine the loading at B and D. Note that the loading on a roller is perpendicular to the surface and that no moment is transferred through the hinges.

$$P^F_{XX} = 0 \qquad P^F_{YY} = -P_{applied}$$

$$P^F_X = P^F_{XX}\,\mathrm{Cos}[\theta_o] + P^F_{YY}\,\mathrm{Sin}[\theta_o] \qquad P^F_Y = -P^F_{XX}\,\mathrm{Sin}[\theta_o] + P^F_{YY}\,\mathrm{Cos}[\theta_o]$$

$$P^C_X = -\phi^C P^C_Y \qquad P^C_Y = \frac{P^F_Y\left(X^F - X^A\right) - P^F_X\left(Y^F - Y^A\right)}{\left(X^C - X^A\right) + \phi^C\left(Y^C - Y^A\right)}$$

$$P^A_X = P^F_X - P^C_X \qquad P^A_Y = P^F_Y - P^C_Y$$

$$P^D_X = -\phi^D P^D_Y$$

$$P^D_Y = \frac{-P^C_Y\left(X^C - X^B\right) + P^C_X\left(Y^C - Y^B\right) - P^A_Y\left(X^A - X^B\right) + P^A_X\left(Y^A - Y^B\right)}{\left(X^D - X^B\right) + \phi^D\left(Y^D - Y^B\right)}$$

$$P^B_X = -P^D_X - P^C_X - P^A_X \qquad P^B_Y = -P^D_Y - P^C_Y - P^A_Y$$

$$P_I = (P^A_Y - P^B_Y)/2 \qquad P_{II} = 2(P^A_Y + P^B_Y)$$

Step 5. Iterate on steps 2-4.
A new displacement is calculated based on the most recent load value, and then a new loading based on the newly calculated displacements. These steps are iterated until all parameters reach a stable value, which normally only takes a few iterations.

Step 6. Calculation of global terms from stabilized values.

Once final values of loading and displacement of the specimen have been determined, these stabilized values can be used to calculate toughness values. The stabilized values can also be transformed into the global coordinate system.

To calculate toughness, the moments at the crack tip applied from the split ends of the beam are calculated and divided into symmetric and unsymmetric loading (M_I and M_{II}, respectively). Assuming superposition of the two modes shown in Figure 1, these moments are used to calculated the Mode I and Mode II components of toughnesses using the appropriate χ corrections. The equations for moment include a term containing ϕ, which is the correction for the shortening of the crack length. This correction is not included in the iterative part of the analysis for two reasons. First it will be relatively small since the deformations are expressed in the specimen coordinate system. Second, including this third-order effect would lead to accounting for the sliding of the rollers on the specimen, which would prove difficult in this type of model. This correction is therefore included as shown here, which should capture the majority of the effect:

$$M_A = X^A\left(1-\frac{8}{30}(\phi^A)^2\right)P_Y^A - Y^A P_X^A \qquad M_B = X^B\left(1-\frac{8}{30}(\phi^B)^2\right)P_Y^B - Y^B P_X^B$$

$$M_I = \frac{M_A - M_B}{2} \qquad M_{II} = \frac{M_A + M_B}{2}$$

$$G_I = \frac{M_I^2}{bEI}\left(1+\frac{\chi h}{a}\right)^2 \qquad G_{II} = \frac{3M_{II}^2}{4bEI}\left(1+0.42\frac{\chi h}{a}\right)^2$$

$$\alpha^A = \phi^A + \theta_o \qquad \alpha^B = \phi^B + \theta_o$$

$$\delta_{ab} = \left(X^A - X^B\right)\mathrm{Sin}\left[\theta_o\right] + \left(Y^A - Y^B\right)\mathrm{Cos}\left[\theta_o\right] - 2h - 2h^*$$

$$\delta = (c + L)\,\mathrm{Tan}(\theta_L) - \delta_{ab}$$

March 13, 2002

The following papers have been DAA approved as Unclassified, Publicly Available documents and are available on the Langley Technical Reports Server (LTRS):

Meeting Presentations:

40th AIAA Aerospace Sciences Meeting & Exhibit; 1/14-17/2002, Reno, NV:
F. Ghaffari, *et al.*: Numerical Viscous Flow Analysis of an Advanced Semispan...
M. Blosser: Investigation of Fundamental Modeling and Thermal Performance Issues...
M.L. Blosser, *et al.*: Advanced Metallic Thermal Protection System Development.
J.T. Dorsey, *et al.*: Metallic Thermal Protection System Technology Development:...
L. Jenkins, *et al.*: Flow Control Device Evaluation for an Internal Flow with an...
C.L. Rumsey, *et al.*: Three-Dimensional Effects on Multi-Element High Lift...
J. Casper, *et al.*: Broadband Noise Predictions Based on a New Aeroacoustic...
L.R. Owens, *et al.*: Reynold Number Effects on the Stability & Control...
C.C. Poteet, *et al.*: Preliminary Thermal-Mechanical Sizing of Metallic TPS:...
C.C Poteet, *et al.*: Improving Metallic Thermal Protection System Hypervelocity...
S.Z.. Pirzadeh, *et al.*: Assessment of the Unstructured Grid Software TetrUSS...
J.A. Dec, *et al.*: Probabilistic Design of a Mars Sample Return Earth Entry...
M. Hemsch: Statistical Analysis of CFD Solutions from the Drag Prediction...
A.D. Cutler, *et al.*: CARS Thermometry in Supersonic Combustor for CFD Code...
Cockrell, *et al.*: Aeroheating Predictions for the X-43 Cowl-Closed Configuration...
W.G. Tomek, *et al.*: Investigation of Reynolds Number Effects on a Generic...
L.M. Hudy, *et al.*: Wall-Pressure-Array Measurements Beneath a Separating...
B.L. Crawford, *et al.*: Results From a Sting Whip Correction Verification Test...
M.P. Hamner, *et al.*: Using Temperature Sensitive Paint.
J. Rocker, *et al.*: Using the Web for Competitive Intelligence (CI) Gathering.

ASTM 14th Symp. on Composite Materials: Testing & Design, 3/11-12/2002, Pittsburgh, PA:
J.R. Reeder: A Criterion to Control Nonlinear Error in the Mixed-Mode...

NOISE-CON 2001, 10/29-31/2001, Portland, ME:
D.A. Senzig; *et al.*: Measured Engine Installation Effects of Four Civil Transport...

4th USA/Europe Air Traffic management R&D Seminar, 12/3-7/2002; Santa Fe, CA:
D.J. Wing, *et al.*: Airborne use of Traffic Intent Information in a Distributed Air...

AHS Structure Specialists; Meeting, 10/30-11/1/2001, Williamsburg, VA:
D.C. Jegley, *et al.*: Evaluation of the Structural Response and Failure of a Full...

20th Digital Avionics Systems Conference, 10/14-18/2001, Daytona Beach, FL:
J.P. Chamberlain, *et al.*: Convective Weather Detection by General Aviation...

3rd Triennial Int'l Fire & Cabin Safety Research Conf., 10/22-25/2001. Atlantic City, NJ:
K.H. Lyle, *et al:* Data Reduction and its Impact on Test-Analysis Correlation.